Mechanical characterization of spark plasma sintered titania-silicon oxycarbide (TiO 2 /SiOC) nanocomposites

E.W. Awin, K.C.H. Kumar, S. Bernard, R. Kumar

Mechanical characterization of spark plasma sintered titania-silicon oxycarbide (TiO_2/SiOC) nanocomposites

Mechanische Charakterisierung von sparkplasmagesinterten Titan-Silcium-Oxidkarbid-Verbundwerkstoffen (TiO_2/SiOC)

E.W. Awin[1], K.C.H. Kumar[1], S. Bernard[2], R. Kumar[1]

In this work, titania-silicon oxycarbide nanocomposites synthesized via the polymer derived ceramics route have been sintered into crack-free monoliths using spark plasma sintering and their mechanical properties as well as their apparent density have been characterized. The x-ray diffractogram clearly showed the stabilization of anatase phase of size less than 10 nm size in an amorphous silicon oxycarbide matrix at 1200 °C. The hardness and elastic modulus determined using nanoindentation were found to be 9 GPa and 82 GPa, respectively, and the fracture toughness calculated using indentation crack length method was found to be 2.34 MPa$m^{1/2}$. In addition to this, ball-on-three ball technique was used to evaluate the biaxial flexural strength and fractographic studies were carried out to understand the fracture mechanisms.

Keywords: Spark plasma sintering **/** Nanoindentation **/** Fracture toughness **/** Ball-on-three ball method

1 Introduction

In recent years, silicon oxycarbide based ceramics have gained a lot of attention in the research community due to their excellent mechanical properties as well as their high chemical and thermal stability [1]. Silicon oxycarbide based ceramics have been synthesized through a wide variety of processing routes, out of which commonly used techniques are the sol-gel and the polymer-derived ceramics route [2, 3]. The main advantage of implementing the polymer derived ceramics route is in the flexibility to control and adapt the structure and the composition of the ceramics for the targeted application based on the chemistry of the selected preceramic polymer as precursor [4]. The development of nanocomposites in which the structure of at least one phase is designed at nanoscale allows improved performance in applications that can reach far beyond those of conventional polymer derived ceramics [5–8]. For example, nano-titania (anatase phase) based silicon oxycarbide ceramics, *i.e.*, titania-silicon oxycarbide nanocomposites, as a material for photocatalytic application has the advantage compared to conventional materials due

[1] Laboratory for High Performance Ceramics, Department of Metallurgic and Materials Engineering, Indian Institute of Technology-Madras (IIT Madras), Chennai, India

[2] Université de Limoges, CNRS, IRCER, UMR 7315, Limoges, France

Corresponding author: R. Kumar, Laboratory for High Performance Ceramics, Department of Metallurgic and Materials Engineering, Indian Institute of Technology-Madras (IIT Madras), Chennai 600036, India,
E-Mail: nvrk@iitm.ac.in

to the combinatorial effect: the silicon oxycarbide phase providing mechanical support whereas titania promoting photocatalysis [9]. However, the mechanical properties of polymer derived ceramics-based nanocomposites have received limited attention so far compared to the photocatalytic aspects.

There have been only very few studies carried out on the mechanical stability of silicon oxycarbide based ceramics. Recently, the dependence of fracture toughness and elastic modulus on the presence of free carbon, crystalline phases of silicon carbide, zirconia and hafnia in silicon oxycarbide based glass-ceramics were reported [10, 11]. The flexural strength data of silicon oxycarbide ceramics was reported to be in the range of 350 MPa–390 MPa [12, 13]. The biaxial flexural strength of a crack-free dense monolith produced by field-assisted sintering was found to be 173 MPa–222 MPa [14]. Recently, studies carried out on the strontium and barium doped silicon oxycarbide ceramics revealed that the initial particle size, as well as the porosity, affects the flexural strength [15, 16]. The biaxial flexural strength for sub-micron sized strontium and barium doped silicon oxycarbide ceramics were reported to be 220 MPa and 209 MPa, respectively.

Lifetime estimation of a material requires the knowledge of its mechanical strength. The conventional test methods such as three and four-point bend tests, ball-on-ring, ring-on-ring test method and pin-on-three balls for determining the mechanical strength of a material have many disadvantages [17]. In the case of three and four-point bending test, the requirement of a large number of samples and its preparation alter the testing surface. On the contrary, in the case of ball-on-ring and pin-on-three ball method, a slight error in the sample geometry and uncertainty in loading could lead to unevenness in load transfer during the test [17–19]. In the present work, a comprehensive mechanical characterization of spark plasma sintered titania-silicon oxycarbide nanocomposites using indentation techniques and ball-on-three ball test was carried out for the first time. In ball-on-three ball tests, the problem associated with the above-mentioned methods is lessened to a large extent.

2 Experimental details

Commercially available polyhydrido methylsiloxane and titanium n-tetra butoxide were taken in equal amount and mixed continuously for 60 min using a magnetic stirrer. The solution was transferred to a horizontal tubular furnace in an alumina boat. The crosslinking was carried out at 300 °C for 2 h and subsequently pyrolyzed at 1200 °C maintaining a heating rate of 5 °C/min and holding time of 5 h in an ambient atmosphere. A foamy structure was obtained, which was crushed using a mortar and pestle and then subjected to spark plasma sintering (Sumitomo Coal Mining Co. Ltd, Japan). A 13 mm diameter die was used for the compaction of powder wherein graphite foils were placed between the die, punch and the powder for the easy passage of electric current. The sintering was performed in vacuum under a constant pressure of 30 MPa. The desired temperature (1200 °C) was attained at a heating rate of 100 °C/min, and dwell duration was 10 min.

The density of the sintered samples was measured using the water displacement method. The thermogravimetric analysis (NETZSCH STA 409, Selb, Germany) was performed in static air flow maintaining a heating rate of 5 °C/min to 1400 °C. The phase evolution and microstructural characterization were done using x-ray diffractometer (Bruker Discover D8, USA) and scanning electron microscope (FEI Quanta 200, USA), respectively. The Raman spectrum (Horiba, Japan) was recorded using a He Ne laser source operating at 488 nm in the range 100 cm^{-1}–4000 cm^{-1}. The fracture toughness of the material was determined using indentation crack length method using Anstis equation (1). A load of 10 kg was applied, and crack length was measured using scanning electron microscope.

$$K_{IC} \quad \ldots 0{:}016 \left(\frac{E}{H}\right)^{0{:}5} \left(\frac{P}{c^{1{:}5}}\right) \qquad (1)$$

where K_{IC} is the fracture toughness ($MPa\,m^{1/2}$), P is the applied load (N), E is the elastic modulus (GPa), H is the hardness (GPa), and c is the radius of the critical crack (μm).

The Poisson's ratio of the samples was determined by a non-destructive ultrasonic pulse echo

method. The longitudinal wave (10 MHz) and shear wave (5 MHz) transducers were used to measure the ultrasonic velocity.

The biaxial flexural strength test was carried out by ball-on-three ball tests with the aid of a universal testing machine (Zwick Z010, Zwick/Roell, Ulm, Germany), *Figure 1*. Three balls were kept at the base on which the sintered sample was placed, and the fourth ball was symmetrically loaded above the specimen. A preload of 5 N was applied before the start of the experiment to retain the balls in position, maintaining crosshead speed and strain rate constant (1 mm/min and 0.001 s^{-1}, respectively). The load was subsequently increased till failure, and this load was used to calculate the biaxial fracture strength.

The ball-on-three ball test was restricted to five samples, and Weibull analysis was performed with these data points (relative humidity = 40 % and temperature = 27 °C). The sample thickness-to-radius ratio, t/R ratio was maintained at 0.25 for all the samples as ball-on-three ball test was proven to be valid in the range ($0.05 < t/R < 0.6$) for ceramics [17]. The sample being too thick or thin, could induce Hertzian contact stress or buckling issues, respectively.

The failure of a brittle material is usually elicited by the largest flaw in the sample volume. The probability of failure, F for a given sample, as portrayed by Weibull analysis is given by the expression

$$F(s; V) = 1 - \exp\left[-\frac{V}{V_0}\left(\frac{s}{s_0}\right)^m\right] \quad (2)$$

where s is the applied stress (MPa), V is the sample volume (m^3), V_0 is the reference volume, s_0 is the stress at which probability of failure is 63 % (characteristic strength) and m is Weibull modulus which depicts the scatter of stress distribution.

The biaxial flexure strength of the sample was calculated from the fracture load using the equation

$$s_{max} = A\frac{P}{t^2} \quad (3)$$

where A is a dimensionless factor which depends on the specimen geometry and Poisson's ratio (#), P is the applied load (N) at failure and t is the thickness (mm) of the sample. The specimen is defined by its radius R, whereas R_a is the radius of the support circle formed by the three balls and R_b is the radius of the balls (8 mm), which is related by $R_a = \frac{2\sqrt{3}}{3} R_b$. The biaxial flexural strength was calculated using a Web-Mathematica tool developed for discs (www.isfk.at/en/960).

3 Results and discussion

The titania-silicon oxycarbide nanocomposite was synthesized through the polymer derived ceramics route as discussed elsewhere [9]. The thermogravimetric curve exhibits three stages of mass loss at 25 °C–250 °C (loss of alcohols and water), 250 °C–450 °C (polymer decomposition) and 450–800 °C (release of hydrogen and methane gases) [9], *Figure 2*a. The titania-silicon oxycarbide nanocomposites were found to amorphous till 1000 °C and further increase in pyrolysis temperature led to the crystallization of anatase phase at 1200 °C; distributed in an amorphous silicon oxycarbide matrix, Figure 2b [9]. The Rietveld refinement (MAUD) performed on the powder sample indicated that the nanocomposite contains 34 wt. % of the anatase phase [9]. The density of the spark plasma sintered sample was determined using the water displace-

Figure 1. Photograph of Zwick Z010 instrument and the schematic of ball-on-three ball set up.

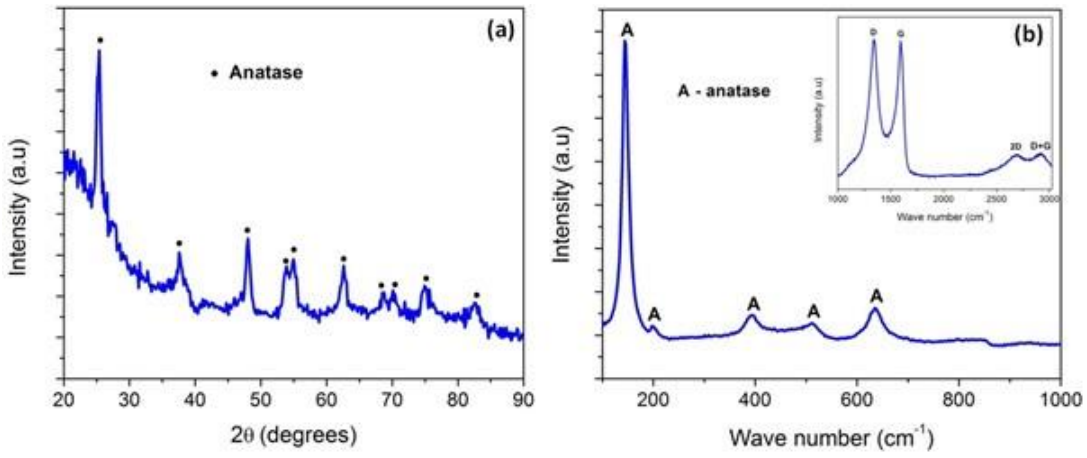

Figure 2. (a) TGA curve indicating the mass loss behavior with respect to temperature (b) X-ray diffractogram indicating the phase evolution of the nanocomposite as a function of pyrolysis temperature (c) X-ray diffractogram of spark plasma sintered nanocomposite revealing the formation of titania and (d) Raman spectra confirming the anatase phase as well as the existence of free carbon.

ment technique (Archimedes principle) and was found to be 2.33 g/cm^3. As inferred from the x-ray diffractogram of the spark plasma sintered sample, the first three dominant peaks at $2\theta = 25.2°$, 47.9° and 37.7° confirm the presence of anatase phase in an amorphous silicon oxycarbide, Figure 2c. A broad hump at 22° indicates the presence of amorphous silica. The crystallite size of anatase was determined using Scherrer's formula and was found to be 9 nm.

The peaks at 145 cm ^{1}, 198 cm ^{1} and 636 cm ^{1} corresponding to E_g band whereas 394 cm ^{1} and 510 cm ^{1} attributing to B_{1g} and $A_{1g} + B_{1g}$ bands, respectively confirms the presence of anatase phase from the Raman spectra, Figure 2d. The inset of Figure 2b clearly presents the D (1343 cm ^{1}) and G (1594 cm ^{1}) peaks of graphitic carbon which relates to the defects and sp^2 hybridized carbon, respectively. The additional peaks observed at 2691 cm ^{1} and 2919 cm ^{1} corresponds to the 2D and D + G bands, respectively.

The scanning electron micrograph of the sintered sample clearly indicated the presence of pores, *Figure 3*. The presence of pores could be attributed to low sintering temperature used in this study.

The elastic modulus and hardness calculated using Oliver and Pharr method were found to be 82 GPa ± 2 GPa and 8.6 GPa ± 0.9 GPa, respectively [20], *Figure 4*a. The hardness values determined using nanoindentation was found to be

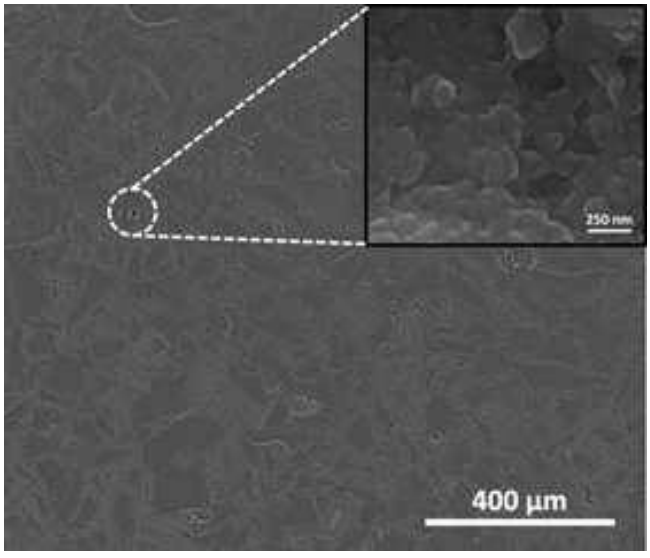

Figure 3. Scanning electron micrograph of the sintered pellet. Inset image shows nanocrystalline grains of titania.

higher when compared to bulk Vickers hardness (5.7 GPa). This could be attributed to the indentation size effect, and the difference in the load applied. The power-law relation as given by the equation (4) was used to fit the unloading segment of the load-displacement curve.

$$P = B(h - h_f)^m \quad (4)$$

where P is the applied load (mN), B&m are fitting parameters, h is the displacement (nm) and h_f is the final indentation depth.

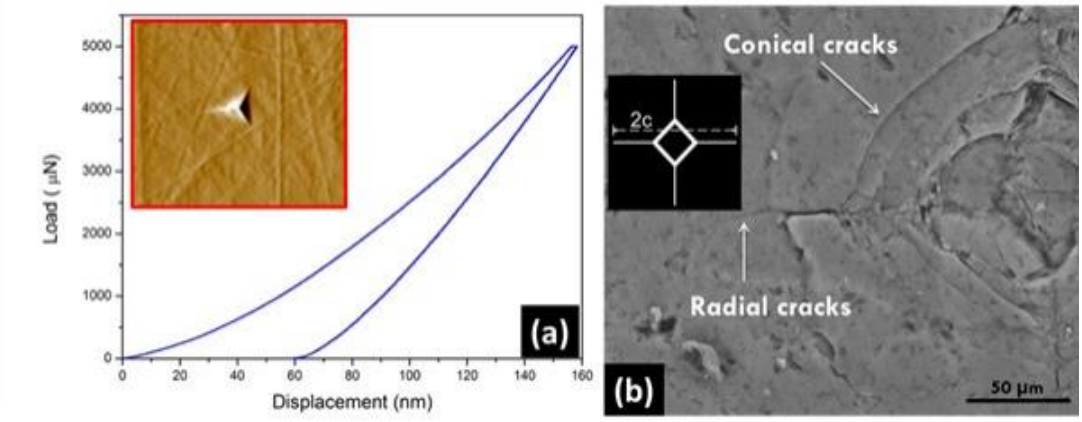

Figure 4. (a) Load vs. displacement curve of titania-silicon oxycarbide nanocomposite (inset image displays the nanoindent impression) and (b) Scanning electron micrograph indicating the evolution of conical and radial cracks.

The power-law index, m was determined to be 1.5 and was analogous to the reported values of polymer derived ceramics [21]. The nanocomposite exhibited considerable elastic recovery (~64 %) during unloading as per the equation (5), which was analogous to the reported values of fused silica [22].

$$\% R \ldots \frac{h_{max} \quad h_f}{h_{max}} \tag{5}$$

The presence of turbostratic carbon at the interphase boundaries between the nanocrystalline titania phases could be attributed to the high elastic recovery in the nanocomposite. The turbostratic carbon is expected to relax upon unloading, causing high elastic recovery. Moreover, in the case of the nanocomposites, the calculated E/H ratio of 9 was comparable to that of fused quartz and silicon oxycarbide implying the ceramic to possess a cracking pattern similar to that of the aforementioned material systems [23]. This also suggests the fact that the uniformly distributed titania nanocrystals in the amorphous silicon oxycarbide matrix have a minimal influence in governing the mechanical properties.

The fracture toughness of the material determined using Anstis equation was found to be 2.34 $MPa\,m^{1/2}$ which was analogous to silicon oxycarbide ceramics [11, 24]. The crack evolution pattern in titania-silicon oxycarbide nanocomposite was comparable to that observed in polymer derived silicon oxycarbide ceramics. The crack pattern observed was a combination of conical and radial crack, Figure. 4b. The investigation performed on the silicon oxycarbide glasses (pyrolyzed at temperatures less than 1000 °C) suggests that the densification of Si O C networks beneath the indenter is responsible for the development of conical cracks. The formation of radial cracks was observed at higher temperatures (>1000 °C) which were attributed to the reduction in the mobility of Si O C network by the covalently bonded carbon atoms. At higher temperatures, the deformation occurs by shear flow rather than by densification under the indenter. The similarity in the structure of titania-silicon oxycarbide nanocomposite to that of silicon oxycarbide, with Si O and Si C could be a reason for the exhibition of mixed conical and radial cracks. In fact, it was also shown that the glass-ceramics possessing high Poisson's ratio (#), # > 0.25 resulted in the formation of radial crack upon indentation. On the contrary, for lower # values (#<0.20), cone cracks were observed [25]. In the current study, the Poisson's ratio of titania-silicon oxycarbide nanocomposite was found to be 0.23. Hence, it could be assumed that the intermediate value of Poisson's ratio might have led to the formation of a combined radial and conical crack.

The Poisson's ratio and elastic modulus were calculated from the following expression, *Table 1*

$$\# \ldots \frac{V_l^2 \quad 2\,V_t^2}{2\,V_l^2 \quad 2\,V^2} \tag{6}$$

t

Table 1. Poisson's ratio and elastic constant of titania-silicon oxycarbide nanocomposite acquired using pulse-echo resonance method.

Sample	Thickness	V_l (m/s)	V_t (m/s)	#	E (GPa)
titania-silicon oxycarbide	3.75	5161	3047	0.23	53.6

$$E \ldots \frac{V_l^2 1 \square 1 \rfloor \quad \#\Rightarrow \square 1}{2\#\Rightarrow \square 1 \quad \#\Rightarrow} \qquad (7)$$

where V_l and V_t are the calculated values of longitudinal and transverse velocities (m/s).

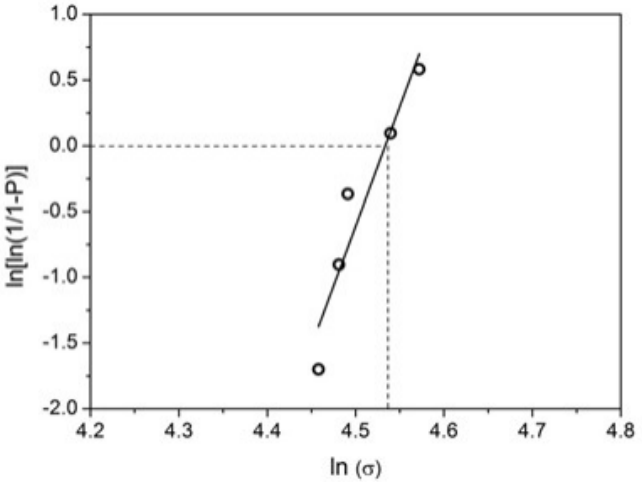

Figure 5. Weibull plot: the probability of failure as a function of failure stress.

The biaxial flexure strength results carried out on the sintered samples as a Weibull diagram. The results are plotted as a function of fracture stress (rearranging) vs. probability of failure (taking the double logarithm of equation 2), *Figure 5*. The Weibull modulus, $m = 18.1 \} 3$ as well as characteristic biaxial flexural strength i.e, probability of failure of 63.21 %, $\sigma_0 = 92.7$ MPa were evaluated according to EN-843-5 [26].

Most of the specimens broke into three pieces whereas in one case, it was observed to fracture into two pieces, *Figure 6*. It is believed that as the strength (stored elastic energy) increases, the number of fracture pieces increases.

The stresses at which sintered samples fractured were in a narrow range, and it can be therefore inferred that this material exhibits high mechanical reliability [25]. The low flexural strength (92.7 MPa) of titania-silicon oxycarbide nanocomposite obtained in this study when compared to its counterpart silicon oxycarbide (153 MPa) could be attributed to the low sintering temperature. The presence of pores would have degraded the flexural strength of the nanocomposite [15]. The influence of free carbon on mechanical properties has always been a subject to controversy. Recently, biaxial flexural strength of 922 MPa was reported for an amorphous silicon oxycarbide ceramic sintered at 1000 °C [27]. The considerable increase in biaxial characteristic stress value has been attributed to the presence of a large amount of free carbon content. On the contrary, a diminution in mechanical properties with an increase in free carbon content was also reported [10]. The density of the sintered sam-

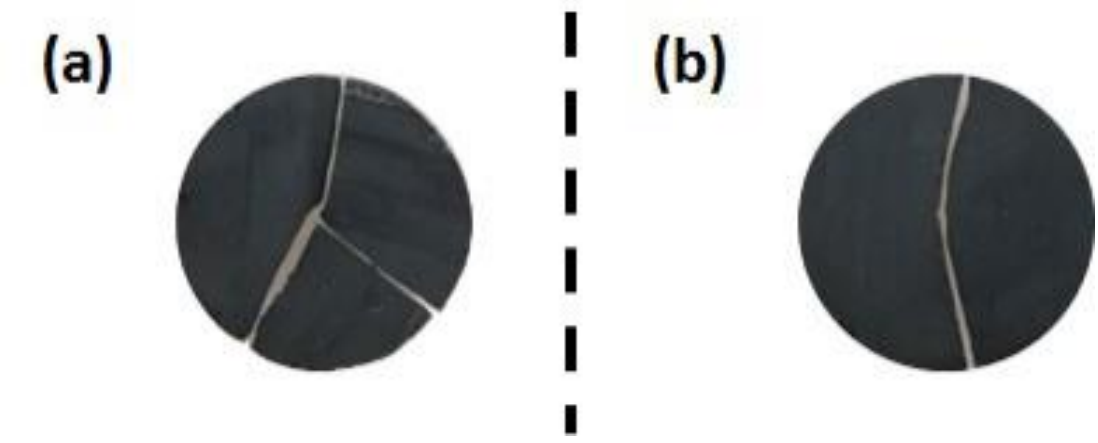

Figure 6. Ball-on-three ball fractured specimens (a) three-fold and (b) two-fold symmetry.

ple was also found to be lower with an increase in free carbon content. Even though, the biaxial stress has no direct repercussion on the values of hardness and elastic modulus, the fact that the free carbon plays a significant role in the densification mechanism; it is believed to lower the biaxial flexural strength of the components. In the present study, the I_D/I_G ratio of 1.008 implies the existence of disordered carbon in the nanocomposite. Hence, it could be inferred that the presence of free carbon could have resulted in the drop of biaxial stress values. It is inferred from the plot of characteristic stress (σ_0) versus Weibull modulus (m) of different ceramic materials and bulk metallic glasses that the titania-silicon oxycarbide nanocomposite exhibits a Weibull modulus value of $m = 18$ are comparable to the values of glass ceramics, alumina/silicon carbide/silicon nitride and zirconia-based ceramics, *Figure 7* [28–31]. Taking into consideration of the characteristic stress value, the titania-silicon oxycarbide nanocomposite was in par with the glass-ceramics. However, the σ_0 was found to be lower than other ceramic-based materials. The high value of m implies that the nanocomposite is reliable for engineering applications.

The polymer derived ceramic approach used for the processing of nanocomposite could result in the formation of pores. The polymer to ceramic conversion happens with the formation of cracks and pores due to the volatilization of low molecular components in the pre-ceramic polymer. The fractographic analysis performed on the ball-on-three ball fractured samples enabled us to identify the origin of fracture, *Figure 8*. The breakage of specimens into fragments and small effective volume to surface ratio makes it difficult to identify the origin of fracture. However, in ball-on-three ball tests, failure is expected to happen at the center of the disc opposite to the loading where the tensile stress is high [32]. From the fractographs, it was clear that the defect present on the surface of the specimen was the reason for failure of many of the samples. The hackle lines (dotted lines) which appear on the fractured surface indicate that fracture has initiated at the surface. The region subjected to the highest tensile stress is shown as dotted box and is expected to be the site of fracture origin, Figure. 8. In all the cases, Type 2 cracks were observed [33]. This could be due to the scratches or pores present on the surface of the specimen, which is substantiated from scanning electron micrographs. When compared to the biaxial flexural strength of the sintered samples, the current material exhibits low values, which could be attributed to the porosity present in the sample. The brittle nature of the sample as well as the porosity, was well understood from the fractographs.

4 Conclusions

The spark plasma sintered titania-silicon oxycarbide nanocomposites synthesized through precursor derived ceramics route resulted in the stabilization of nanocrystalline anatase phase in an

Figure 7. Characteristic stress of different ceramic based materials as a function of Weibull modulus.

Figure 8. Fractograph of the ball-on-three ball samples indicating the area subjected to high tensile stresses (dotted box) and hackle lines (dotted lines) indicating the origin of failure.

amorphous silicon oxycarbide matrix at a temperature as high as 1200 °C. The presence of free carbon was revealed by Raman spectra, and the microstructural characterization confirmed the presence of pores. The hardness and elastic modulus determined using nanoindentation exhibited lower values than expected, which could be attributed to the lower sintering temperature, in turn affecting the densification process. The fracture toughness was calculated using indentation crack length method and the cracking pattern observed was a combination of conical and radial cracks suggesting the deformation was prominently due to shear flow under the indenter. The low value of biaxial flexural strength determined using ball-on-three ball test clearly indicates the effect of porosity and the high Weibull modulus value reciprocates the mechanical stability in the design point of view.

Acknowledgements

We would like to acknowledge the funding received from Indo-French Centre for the Promotion of Advanced Research (IFCPAR/CEFIPRA), a bilateral Indo-French project (Project No. 5108-1) to carry out this work.

5 References

[1] E. Bernardo, P. Colombo, E. Manias, *Ceram. Int.* **2006**, *32*, 679.
[2] G.D. Sorarù, D. Suttor, *J. Sol-Gel Sci. Technol.* **1999**, *14*, 69.
[3] G. Mera, A. Navrotsky, S. Sen, H.J. Kleebe, R. Riedel, *J. Mater. Chem. A* **2013**, *1*, 3826.
[4] P. Colombo, G. Mera, R. Riedel, G.D. Sorarù, *J. Am. Ceram. Soc.* **2010**, *93*, 1805.
[5] E. Ionescu, H.J. Kleebe, R. Riedel, *Chem. Soc. Rev.* **2012**, *41*, 5032.
[6] M.C. Bechelany, V. Proust, C. Gervais, R. Ghisleni, S. Bernard, P. Miele, *Adv. Mater.* **2014**, *26*, 6548.
[7] M. Zaheer, T. Schmalz, G. Motz, R. Kempe, *Chem. Soc. Rev.* **2012**, *41*, 5102.
[8] G. Mera, M. Gallei, S. Bernard, E. Ionescu, *Nanomaterials.* **2015**, *5*, 468.
[9] E.W. Awin, A. Lale, K.C. Nair Hari Kumar, U.B. Demirci, S. Bernard, R. Kumar, *Materials (Basel).* **2018**, *11*.
[10] G.D. Sorarù, L. Kundanati, B. Santhosh, N. Pugno, *J. Am. Ceram. So* **2018**, *102*, 907.
[11] T. To, C. Stabler, E. Ionescu, R. Riedel, F. Célarié, T. Rouxel, *J. Am. Ceram. Soc.* **2020**, *103*, 491.
[12] G.D. Soraru, E. Dallapiccola, G. D. Andrea, *J. Am. Ceram. Soc.* **1996**, *79*, 2074.
[13] G.M. Renlund, S. Prochazka, R.H. Doremus, *J. Mater. Res.* **1991**, *6*, 2723.
[14] M. Esfehanian, R. Oberacker, T. Fett, M.J. Hoffmann, *J. Am. Ceram. Soc.* **2008**, *91*, 3803.
[15] J.H. Eom, Y.W. Kim, *J. Korean Ceram. Soc.* **2015**, *52*, 61.
[16] J.-H. Eom, Y.-W. Kim, *Nippon Seramikkusu Kyokai Gakujutsu Ronbunshi/Journal Ceram. Soc. Japan* **2015**, *123*.
[17] A. Borger, P. Supancic, R. Danzer, *J. Eur. Ceram. Soc.* **2002**, *22*, 1425.
[18] A. Börger, P. Supancic, R. Danzer, *J. Eur. Ceram. Soc.* **2004**, *24*, 2917.
[19] R. Danzer, W. Harrer, P. Supancic, T. Lube, Z. Wang, A. Börger, *J. Eur. Ceram. Soc.* **2007**, *27*, 1481.
[20] W.C. Oliver, G.M. Pharr, *J. Mater. Res.* **1992**, 7, 1564.
[21] R. Sujith, R. Kumar, *Ceram. Int.* **2013**, *39*, 9743.
[22] M.T. Attaf, *Mater. Lett.* **2003**, *57*, 4684.
[23] R. Sujith, A. Zimmermann, R. Kumar, *Adv. Eng. Mater.* **2015**, *17*, 1265.
[24] G.R. Antis, P. Chantikul, B.R.R. Lawn, D.B. Marshall, *J. Am. Ceram. Soc.* **1981**, *46*, 533.
[25] S. Walter, G.D. Soraru, H. Bréquel, S. Enzo, *J. Eur. Ceram. Soc.* **2002**, *22*, 2389.
[26] T. European, P. Env, S. Standard, S. Standards, T. Cata, *E. Standards* **1996**.
[27] P.V.W. Sasikumar, G. Blugan, N. Casati, E. Kakkava, G. Panusa, D. Psaltis, J. Kuebler, *Ceram. Int.* **2018**, *44*, 20961.
[28] W. Harrer, R. Danzer, A. Rendtel, *J. Eur. Ceram. Soc.* **2016**, *36*, 3895.
[29] S. Rasche, S. Strobl, M. Kuna, R. Bermejo, T. Lube, *Procedia Mater. Sci.* **2014**, *3*, 961.

[30] S. Strobl, T. Lube, P. Supancic, M. Stoiser, O. Schöppl, R. Danzer, *J. Eur. Ceram. Soc.* **2014**, *34*, 4167.
[31] W. Harrer, M. Schwentenwein, T. Lube, R. Danzer, *J. Eur. Ceram. Soc.* **2017**, *37*, 4331.
[32] W. Harrer, R. Danzer, P. Supancic, T. Lube, *Key Eng. Mater.* **2009**, *409*, 176.
[33] W. Harrer, R. Morrell, R. Danzer, *J. Eur. Ceram. Soc.* **2014**, *34*, 3283.

Received in final form: September 28th 2021